Application of Homogeneously Precipitated Nanosized Fe-Doped Alumina Powders to Carbon Nanotube Growth

Yasemin Çelik and Ender Suvacı*,†

Department of Materials Science and Engineering, Anadolu University, 26480 Eskisehir, Turkey

Emmanuel Flahaut,‡,§ Alicia Weibel,‡ and Alain Peigney‡,*

‡Université de Toulouse, UPS, INP, Institut Carnot Cirimat, 118, route de Narbonne, F-31062 Toulouse cedex 9, France

§CNRS, Institut Carnot Cirimat, F-31062 Toulouse, France

Homogeneous precipitation of hydroxides was investigated as an alternative method to synthesize Fe-doped aluminum oxide (α-$Al_{2-2x}Fe_{2x}O_3$) particles over which carbon nanotubes (CNTs) were grown via a catalytic chemical vapor deposition (CCVD) method. Performance of the homogeneously precipitated particles for CNT growth was quantitatively compared with that of the combustion-synthesized particles. The main advantage of the homogeneous precipitation of hydroxides and subsequent calcination process against to the combustion synthesis and other commonly practiced chemical routes is the ability to tailor the Fe-doped Al_2O_3 precursor powder characteristics such as size and specific surface area (SSA) without requiring any milling step and also to control the phase composition of the oxide powder with high Fe content, and subsequently the quality and quantity of CNTs during CCVD process. The particle size of the precipitated and calcined α-$Al_{2-2x}Fe_{2x}O_3$ powders varies between ~50 and 400 nm for 5–10 cat.% Fe-containing systems. The monodispersed particle size distribution and optimum phase composition of the homogeneously precipitated powders, particularly for a 10 cat.% Fe content in the starting oxide, and their much higher SSA than similar materials prepared by other chemical routes lead to production of high amounts of good quality CNTs.

I. Introduction

Carbon nanotubes (CNTs) are very promising materials in the field of nanotechnology due to their unique and exceptional properties.[1] Therefore, they can find many applications, such as in electronic devices and their incorporation in polymer–matrix, metal–matrix, or ceramic–matrix composites.[2] The obtained nanocomposites generally exhibit improved electrical and/or mechanical properties.[3,4] The main difficulty to prepare a nanocomposite is to achieve a homogeneous dispersion of the CNTs in the matrix.

Mechanical mixing and chemical methods are the common approaches that have been utilized for dispersion of CNTs.[4,5] Both of these methods allow to select the type and purity of CNTs before the dispersion process. However, such methods bring some potential hazard issues due to handling free CNTs. The mixing of CNTs with the ceramic powders by comilling processing requires long times and usually damages the CNTs[5] and aggressive chemical functionalization may introduce structural defects in nanotubes.[5] An alternative to these methods is synthesis of CNTs on the surface of ceramic particles.[4] Peigney *et al.*[6] have developed a catalytic route for the *in situ* formation of CNTs over a composite Fe–Al_2O_3 powder by reduction of an alumina–hematite solid solution powder in H_2–CH_4 atmosphere. This simple and scalable technique can be applied to a wide range of matrices[4] and provides a very homogeneous dispersion of CNTs in the CNTs–Fe–Al_2O_3 nanocomposite powder, while avoiding the hazardous effect of free CNTs. Previous studies showed that, in order to obtain a noteworthy amount of CNTs with a good quality in the nanocomposite powder system, the starting oxide powder should be crystallized in the stable, monophased α-form (Fe-doped aluminum oxide (α-$Al_{2-2x}Fe_{2x}O_3$))[7,8] and have a very high specific surface area (SSA).[9] Moreover, increasing Fe content in the starting oxide powder provides more catalytic particles available for CNTs growth.[8] However, α-Fe_2O_3 (hematite) phase segregation, which results in the formation of carbon nanofibers (CNFs), should be avoided in the catalytic materials to be utilized for CNTs synthesis,[8] although α-Fe_2O_3 may lead to smaller particle-sized corundum (α-Al_2O_3) by lowering the γ to α-Al_2O_3 transformation temperature.[10,11] In previous works, the alumina–hematite starting powders for CNT synthesis have been mostly prepared by the mixed-oxalate,[6–9] oxinate,[12] and combustion routes[13] with maximum Fe content of alumina $\leq$10 cat.% (i.e., $x \leq 0.1$ in $Al_{2-2x}Fe_{2x}O_3$). Unfortunately, the reported SSA values for the calcined α-$Al_{2-2x}Fe_{2x}O_3$ powders prepared by these methods are relatively low (<10 m^2/g), which is a limiting factor for the production of large amount of CNTs over the Fe–Al_2O_3 composite powders. Consequently, the synthesis of monophased α-$Al_{2-2x}Fe_{2x}O_3$ powders with high SSA (i.e., >10 m^2/g) remains a challenge in order to obtain higher amount of good quality *in situ* synthesized CNTs over alumina matrix nanocomposite powders.

Homogeneous precipitation from aqueous salt solutions in the presence of a precipitating agent has been demonstrated as a simple and effective method for the production of metal hydroxide particles with controllable size and shape.[14] The slow and uniform release of the precipitating agent in the reaction mixture allows production of dense and pure particles with uniform size distribution as well as tailorability of the surface area. The research objective of this study was to investigate the homogeneous precipitation of hydroxides as an alternative method for the preparation of Fe-doped alumina powders (α-$Al_{2-2x}Fe_{2x}O_3$, $x \leq 0.1$) for the CNTs–Fe–Al_2O_3 nanocomposite powder manufacturing.

Presented at the 10th International Conference and Exhibition of the European Ceramic Society, Berlin, June 19, 2007.

Based in part on the thesis submitted by Y. (Bozkaya) Celik for the M.S. degree in nanotechnology programme, Anadolu University, 2008.

The financial support for this study by The Scientific and Technological Research Council of Turkey (TUBITAK) under the contract number 106M543 and Centre National de la Recherche Scientifique (CNRS) under the contract number 20223.

*Member, The American Ceramic Society.

†Author to whom correspondence should be addressed. e-mail: esuvaci@anadolu.edu.tr

II. Experimental Procedure

(1) Preparation of α-$Al_{2-2x}Fe_{2x}O_3$ Powders

In this study, aqueous solutions of aluminum sulfate octadecahydrate ($Al_2(SO_4)_3 \cdot 18H_2O$, Merck (Darmstadt, Germany), extra pure) and iron(III) nitrate nonahydrate ($Fe(NO_3)_3 \cdot 9H_2O$, Merck, GR for analysis) were prepared with varying molarities depending on aluminum and iron fractions in the target solid solutions. 0.05*M* $Al_2(SO_4)_3 \cdot 18H_2O$ and required amount of $Fe(NO_3)_3 \cdot 9H_2O$ were dissolved in distilled water separately and then mixed together in a beaker. pH was decreased to 2.0 by addition of 5 wt.% HNO_3 aqueous solution. The solution was heated while it was being stirred at ~600 rpm. When the temperature of the solution reached 70°C, hexamethylene tetramine ($C_6H_{12}N_4$, HMT) was added and some turbidity, indicating the formation of particles, was immediately observed in the solution. The system was heated to 90°C for the complete activation of HMT. After stirring the suspension for 1.5 h at 90°C, the supernatant was removed by centrifugation; this step was repeated five times by refreshing the distilled water. The powders were then dried in a freeze-dryer. Thermogravimetric analysis and differential thermal analysis (DTA) were performed to determine the calcination temperature of the as-synthesized powders to obtain a stable α-phase. Accordingly, the powders were heated in laboratory air at 5°C/min up to 1000°C ≤ *T* ≤ 1070°C. They were held at these temperatures for 1–60 min. The amount of the powder that was obtained after calcination is ~0.5 g for each batch. Calcined solid solutions were denoted as *w*Fe*y*T*z*t, where *w*, *y*, and *z* refer to the cationic percent of Fe in the $Al_{2-2x}Fe_{2x}O_3$ ($x = 0.05$, 0.07, and 0.10), calcination temperature (°C), and calcination time (minute) of the starting oxide powders, respectively.

In order to compare efficiency of the homogeneously precipitated powders for CNTs synthesis, $Al_{1.8}Fe_{0.2}O_3$ (10 cat.% Fe-doped) powder was also produced by combustion route, which was described in detail by Cordier *et al.*[13] In this process, the required proportion of aluminum nitrate nonahydrate ($Al(NO_3)_3 \cdot 9H_2O$, Merck, extra pure) and iron nitrate nonahydrate ($Fe(NO_3)_3 \cdot 9H_2O$, Merck, GR for analysis) were dissolved in distilled water in a Pyrex® beaker. A mixture of citric acid and urea (75% citric acid and 25% urea) was used as fuel, in a quantity equal to twice the stoichiometric ratio.[13] The required amount of citric acid and urea were dissolved in distilled water and then added into the nitrate solution. The solution was stirred at 600 rpm and ca. 120°C for 1 h. The Pyrex® beaker was then placed in a preheated furnace, at 550°C, and kept there for at least 20 min. The as-synthesized amorphous powder was subjected to two-stage calcination process: it was first heated at 5°C/min up to 600°C, 1.5 h of dwell time in order to remove the residual carbon and then at 15°C/min up to 1100°C, 20 min of dwell time to obtain the α-phase. It is possible to produce up to 4 g of calcined powder for each batch with the conditions utilized in this study. After calcination, the powder (~25 g of batch) was attrition milled at 250 rpm for 4 h in distilled water by using ~480 g of yttria-stabilized ZrO_2 balls, 3 mm in diameter. The calcined and attrition milled $Al_{1.8}Fe_{0.2}O_3$ solid solution powder obtained by the combustion route is denoted as CS throughout the text.

(2) Production of CNT–Fe–Al_2O_3 Nanocomposite Powders

The prepared powders were placed in alumina boats in the middle of a catalytic chemical vapor deposition (CCVD) chamber and then reduced in H_2–CH_4 gas mixture (82 mol% H_2 as reducing gas and 18 mol% CH_4 as carbon source) at 1000°C with a heating and cooling rate of 5°/min (no dwell) to produce CNTs–Fe–Al_2O_3 nanocomposite powders.[15,16] These nanocomposite powders are presented with an "R" at the beginning of the initial code of the sample, i.e., R–*w*Fe*y*T*z*t or R–CS.

(3) Characterization

To determine the temperature of the exothermic transformation from the cubic phase to the stable α-form, DTA were performed in air up to 1200°C with a heating rate of 10°C/min on the homogeneously precipitated powders. Phase analyses of the powders were performed by XRD (Rigaku Rint 2200, Tokyo, Japan) with Cu*K*α radiation. To get additional information about the substitution of Al^{3+} by Fe^{3+} cations as a function of Fe content and calcination temperature and/or time, the cell parameters were determined from the XRD data using silicon as a reference standard. The morphology of the as-synthesized and calcined powders was examined by field-emission-gun scanning electron microscopy (FEG-SEM, Zeiss Supra 50 VP, Oberkochen, Germany). The SSA of the $Al_{2-2x}Fe_{2x}O_3$ powders (S_i) was measured by Brunauer–Emmett–Teller (BET) method (Micromeritics FlowSorb II 2300, Micromeritics Instrument Corporation, Norcross, GA) using N_2 adsorption at liquid N_2 temperature. The accuracy of the measurements is estimated to be ±3%. Effects of the calcination temperature and time on the SSA of the obtained α-$Al_{2-2x}Fe_{2x}O_3$ powders and role of the SSA of these powders on CNTs synthesis were investigated. In addition to BET, the crystallite size of the α-$Al_{2-2x}Fe_{2x}O_3$ powders were determined according to Scherrer's equation[17] via an X-ray based calculation and the corresponding SSA values were calculated assuming the particles as equivalent spheres. In the calculations, *(01–12)* peak of corundum was utilized as reference peak while *(111)* peak of silicon was used for correction as internal standard.

The CNTs–Fe–Al_2O_3 nanocomposite powders were characterized by FEG-SEM (Jeol JSM 6700F, Tokyo, Japan). Carbon content analysis and SSA measurements were carried out in order to get quantitative data about CNTs synthesis efficiency. The carbon content (C_n) of the nanocomposites, which shows the amount of carbon species deposited during CCVD, was determined by flash combustion method with an accuracy of ±2%. The SSA of the CNTs–Fe–Al_2O_3 nanocomposite powders (S_n) were measured by the BET method. Then, the nanocomposites were oxidized at 900°C for 2 h in order to remove all carbon species and the SSA of the oxidized powders (S_o) was measured. These results were then used for calculating the parameters representing the quantity (ΔS, $\Delta S = S_n - S_o$) and the quality ($\Delta S/C_n$) of the CNTs.[6] The CNTs–Fe–Al_2O_3 nanocomposite powders were also characterized by Raman spectroscopy and transmission electron microscopy (TEM). The Raman spectra were recorded at 632.82 nm and 7 mW using a DilorXY (JY Inc., Edison, NJ) micro-Raman set-up with back-scattering geometry. TEM analyses were performed on the CNTs–Fe–Al_2O_3 nanocomposite powders with a Jeol JSM 1011 operated at 100 kV. The samples were prepared by sonicating the nanocomposite powder in ethanol and then dropping that suspension on a copper grid coated with a lacey carbon film.

III. Results

(1) Oxide Powders Produced by Homogeneous Precipitation and Calcination

DTA results (not shown) revealed that the transition from cubic to corundum phase occurs at 1105°, 1070°, and 1050°C for the powders containing 5, 7, and 10 cat.% Fe, respectively. The decrease in the transformation temperature into stable form with increasing Fe content is in agreement with the previous studies.[10,11] Accordingly, to complete the transformation of the precipitated powders into the corundum phase as well as maintaining high SSA, the powders were heat treated at 10°–50°C below these transformation temperatures for some period of time (Table I).

Figure 1(a) shows the effect of Fe content on the phase development of 5Fe1050T60t, 7Fe1050T60t, and 10Fe1050T60t powders. A shift of the main peak positions toward lower 2θ values with respect to pure α-Al_2O_3, indicates substitution of Al^{3+} cations by Fe^{3+} in the corundum lattice to form an α-$Al_{2-2x}Fe_{2x}O_3$ solid solution. Furthermore, this shift increases with increasing Fe content. Besides the α-$Al_{2-2x}Fe_{2x}O_3$ peaks, hematite-rich secondary phase is detected for the 10Fe1050T60t powder. As the Fe content is decreased to 7 and 5 cat.%, no

Table I. Some Characteristics of the Calcined $Al_{2-2x}Fe_{2x}O_3$ Powders Produced by Homogeneous Precipitation Method and of the Carbon Nanotube–Fe–Al_2O_3 Nanocomposite Powders

Powder composition	Calcination: T (°C), t (minutes)	Powder code	Composite code	S_i[†] (m^2/g)	S_n[‡] (m^2/g)	S_o[§] (m^2/g)	ΔS[¶] (m^2/g)	C_n[‖] (wt%)	$\Delta S/C_n$[**] (m^2/g)
$Al_{1.8}Fe_{0.2}O_3$	1000, 1	10Fe1000T1t	R–10Fe1000T1t	38.7±1.2	53.9±1.6	31.1±0.9	22.8±2.5	13.9±0.3	164±21
$Al_{1.8}Fe_{0.2}O_3$	1000, 30	10Fe1000T30t	R–10Fe1000T30t	19.1±0.6	46.0±1.4	15.1±0.5	30.9±1.9	9.4±0.2	329±27
$Al_{1.8}Fe_{0.2}O_3$	1050, 60	10Fe1050T60t	R–10Fe1050T60t	12.9±0.4	33.9±1.0	13.0±0.4	20.9±1.4	12.4±0.3	169±15
$Al_{1.86}Fe_{0.14}O_3$	1060, 60	7Fe1060T60t	R–7Fe1060T60t	29.3±0.9	45.0±1.4	28.5±0.9	16.5±2.3	7.3±0.2	227±36
$Al_{1.9}Fe_{0.1}O_3$	1070, 60	5Fe1070T60t	R–5Fe1070T60t	34.0±1.0	48.8±1.5	30.0±0.9	18.8±2.4	9.4±0.2	200±30
$Al_{1.8}Fe_{0.2}O_3$[††]	1100, 20	CS	R–CS	32.9±1.0	48.6±1.5	11.0±0.3	37.6±1.8	8.2±0.2	459±31

[†]Specific surface area of the calcined $Al_{2-2x}Fe_{2x}O_3$ powder. [‡]Specific surface area of the nanocomposite powder. [§]Specific surface area of the powder oxidized at 900°C. [¶]Represents the quantity of carbon nanotubes ($\Delta S = S_n - S_o$). [‖]Carbon content of the nanocomposite powder. [**]Represents the quality of carbon nanotubes. [††]$Al_{1.8}Fe_{0.2}O_3$ powder prepared by combustion synthesis and subsequently attrition milling.

α-Fe_2O_3 peaks are observed. However, broad peaks of transition (γ or θ) Al_2O_3 phase appears in this case, probably due to insufficient calcination temperature and/or time (Fig. 1(a)). Increasing the calcination temperature of 5 cat.% Fe-doped powder to 1070°C allowed obtaining a monophased α-$Al_{1.9}Fe_{0.1}O_3$ powder with neither transitional alumina- nor hematite-rich phases (Fig. 1(b)), while α-Fe_2O_3 peak was detected in 7 cat.% Fe-doped powder when its calcination temperature was increased to 1060°C. Figure 1(c) shows the XRD patterns of 10 cat.% Fe-doped powders, which were calcined at 1000°C for 1 and 30 min. It is observed that both powders contain hematite-rich secondary phase. Additionally, the powder calcined for 1 min (10Fe1000T1t) contains transitional Al_2O_3 phase. The XRD pattern of the CS powder (10 cat.% Fe-doped) synthesized by the combustion route and calcined at 1100°C, 20 min (Fig. 1(d)), revealed only the peaks of α-$Al_{1.8}Fe_{0.2}O_3$.

The cell parameter calculations (Table II) showed that the c parameter of 10 cat.% Fe-doped powders increased with increasing calcination time up to 30 min, indicating substitution of more Al^{3+} cations by Fe^{3+}, as in agreement with the shift observed in the XRD patterns. The c parameters for 10Fe1000T30t and 10Fe1050T60t are similar. This suggests that the amount of Fe_2O_3 dissolved in the Fe-doped Al_2O_3 matrix reaches a saturation value after calcination at 1000°C for 30 min. However, further analysis is required to test this hypothesis. The 10Fe1000T1t powder contains some transition Al_2O_3 phase, therefore, cell parameter measurements may not give reliable results. The 5Fe1070T60t powder has a lower c parameter than the 10 cat.% Fe-doped powders, due to lower Fe content. The c parameter of the CS powder is higher than homogeneously precipitated powders as expected, because no α-Fe_2O_3 peak (i.e., all Fe is distributed in the alpha alumina lattice) was detected in its XRD pattern. The higher solubility of iron in alumina for the

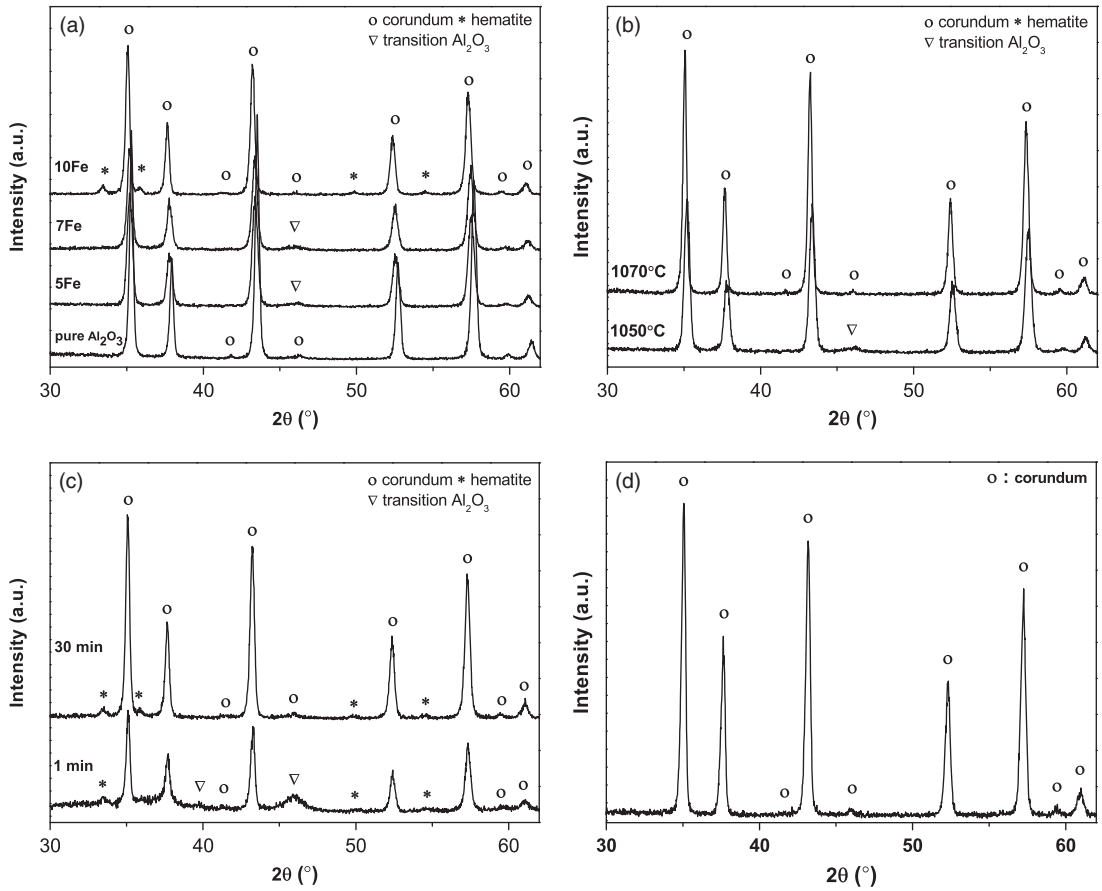

Fig. 1. XRD patterns of homogeneously precipitated $Al_{2-2x}Fe_{2x}O_3$ powders showing the effect of (a) Fe content (the powders were calcined at 1050°C for 60 min), (b) calcination temperature (5Fe1050T60t and 5Fe1070T60t), and (c) calcination time (10Fe1000T1t and 10Fe1000T30t) on the phase development. (d) XRD pattern of CS powder (combustion-synthesized $Al_{1.8}Fe_{0.2}O_3$ powder calcined at 1100°C for 20 min and then attrition milled).

Table II. Cell Parameter Values (nm) of Calcined Fe-Doped Alumina Powders

	5Fe1070T60t	10Fe1000T1t	10Fe1000T30t	10Fe1050T60t	CS	Corundum	Hematite
c	1.3023	1.3028	1.3042	1.3044	1.3063	1.2991	1.3749

Data for corundum and hematite were taken from JCPDS Files No. 10-173 and No. 33-664, respectively.

CS powder could arise from the faster reaction kinetics during combustion synthesis, which allows the production of a metastable solid solution.

The SSA (S_i, Table I) of the 10 cat.% Fe-doped Al_2O_3 powders decreases with increasing calcination temperature and/or time (38.7, 19.1, and 12.9 m^2/g for 10Fe1000T1t, 10Fe1000T30t, and 10Fe1050T60t, respectively). The exceptionally high S_i value of the 10Fe1000T1t arises probably from the presence of transitional Al_2O_3 phase. Surprisingly, it is observed that the SSA of the $Al_{2-2x}Fe_{2x}O_3$ powders increases with simultaneously increasing the calcination temperature and decreasing the Fe content (12.9, 29.3, and 34.0 m^2/g for 10Fe1050T60t, 7Fe1060T60t, and 5Fe1070T60t, respectively). These results can be attributed to the reduction in the Fe content, which shifts the crystallization of the solid solution toward higher temperatures. The SSA measurements of the 5 and 10 cat.% Fe-doped alumina powders, which were calcined at 1050°C for 60 min, show that the SSA increases with decreasing Fe content. The SSA values of 10Fe1050T60t and 5Fe1050T60t powders are 12.9 and 31.9 m^2/g, respectively. The CS powder, after calcination at 1100°C for 20 min, exhibits much lower SSA ($\sim$3 m^2/g) with respect to the calcined homogeneously precipitated powders. Therefore, a subsequent attrition milling was applied to the CS powder after its calcination, and its surface area was thus increased up to 32.9 m^2/g.

The XRD-based crystallite size values, which are 42.0, 47.4, and 52.0 nm for the 10Fe1000T1t, 10Fe1000T30t, and 10Fe1050T60t, respectively, show an increase with increasing calcination temperature and/or time. The corresponding SSA values (34.6, 30.7, and 27.4 m^2/g for the 10Fe1000T1t, 10Fe1000T30t, and 10Fe1050T60t, respectively) calculated from the crystallite sizes show a decreasing trend with increasing calcination temperature and/or time as in agreement with the SSA values (38.7, 19.1, and 12.9 m^2/g, respectively) measured by BET method. The difference between the calculated and measured SSA values of the 10Fe1000T30t and 10Fe1050T60t probably arises from neck formation (i.e., the first stage of sintering) between particles during the calcination process, which causes a lower SSA in BET. The crystallite size of 5Fe1070T60t (39.7 nm) is smaller than that of 10 cat.% Fe-doped powders, although it was calcined at a higher temperature. The calculated SSA (37.3 m^2/g) of the 5Fe1070T60t is very close to the measured value (34.0 m^2/g).

The SEM image of the 10Fe1000T30t powder (Fig. 2(a)) shows the spherical, nanosized Fe-doped Al_2O_3 particles that range between $\sim$50 and 200 nm in diameter, more or less aggregated due to partial sintering during the calcination process. Because the primary particle size was small enough, no subsequent milling step was applied to the calcined homogeneously precipitated powders. The SEM image of the CS powder (Fig. 2(b)) reveals a wider particle size distribution, from 100 nm to $\sim$1.5 μm. The milling parameters used for this powder seem to be a good compromise to obtain a large SSA (32.9 m^2/g).

(2) CNTs–Fe–Al_2O_3 Nanocomposite Powders

The SEM images of the CNTs–Fe–Al_2O_3 nanocomposite powders show the CNTs and/or the CNTs bundles covering the matrix particles evenly (Fig. 3). In the 5Fe1070T60t system (Fig. 3(a) and (b)), CNTs are either individual or in very small diameter bundles and the quantity remains low in spite of the high SSA of the starting powder. There is a clear increase in the amount of CNTs, and in the diameter of CNTs bundles, as the Fe content in the starting oxide increases from 5 to 7 cat.% and then to 10 cat.% (Figs. 3(a), (c), and (e)). No CNF was detected in the R–5Fe1070T60t (Figs. 3(a) and (b)), while a few CNFs were observed in the R–7Fe1060T60t (Fig. 3(d)) and R–10Fe1000T30t (Fig. 3(e)) systems. Higher amounts of CNFs and carbon nanoribbons (CNRs) were observed both in the R–10Fe1000T1t (Fig. 3(g)) and R–10Fe1050T60t (Fig. 3(h)). In the former system (Fig. 3(g)), CNFs and CNRs form large aggregates in some regions of the powder. Similar to the R–5Fe1070T60t system, no CNF was detected in the SEM micrograph of the R–CS powder (Fig. 4).

The SEM observations provide only qualitative information about the CNTs and/or other forms of carbon such as CNFs in the nanocomposites. Therefore, to analyze such characteristics quantitatively, carbon content (C_n) analyses and SSA measurements were performed on the following nanocomposite powder systems; R–5Fe1070T60t, R–7Fe1060T60t, R–10Fe1000T1t, R–10Fe1000T30t, R–10Fe1050T60t, and R–CS. The C_n analyses results, which range between 7.3 and 13.9 wt.%, are summarized in Table I.

The SSA of the nanocomposite powders (S_n, Table I) increased severely after being subjected to the CCVD. The SSA values of the R–10Fe1000T1t, R–10Fe1000T30t, and R–5Fe1070T60t powders after elimination all the carbon species via oxidation (31.1, 15.1, and 30.0 m^2/g, respectively) are lower than the initial surface area of the corresponding starting oxides (S_i: 38.7, 19.1, and 34.0 m^2/g, respectively). The SSA of R–CS

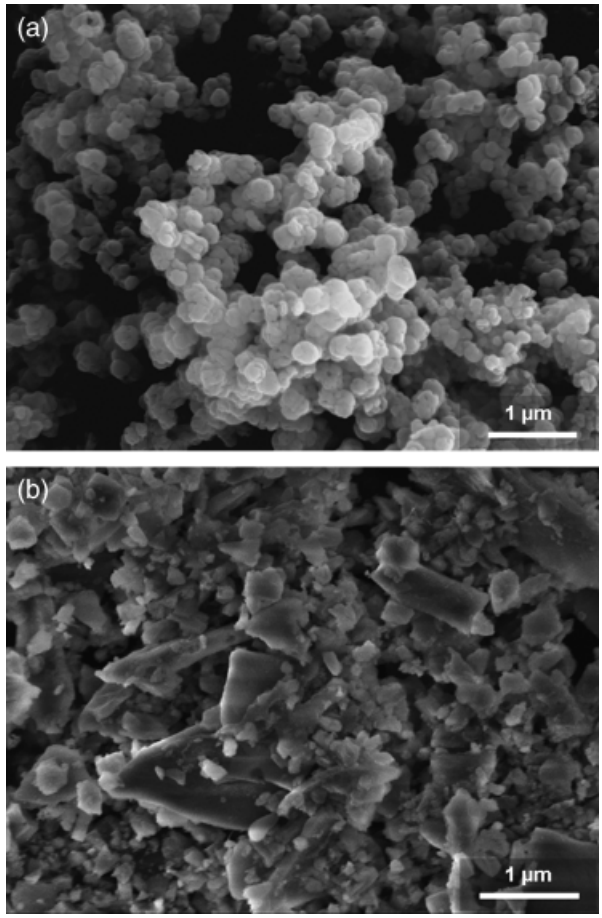

Fig. 2. SEM micrographs of (a) the homogeneously precipitated and calcined 10Fe1000T30t and (b) the combustion-synthesized powders.

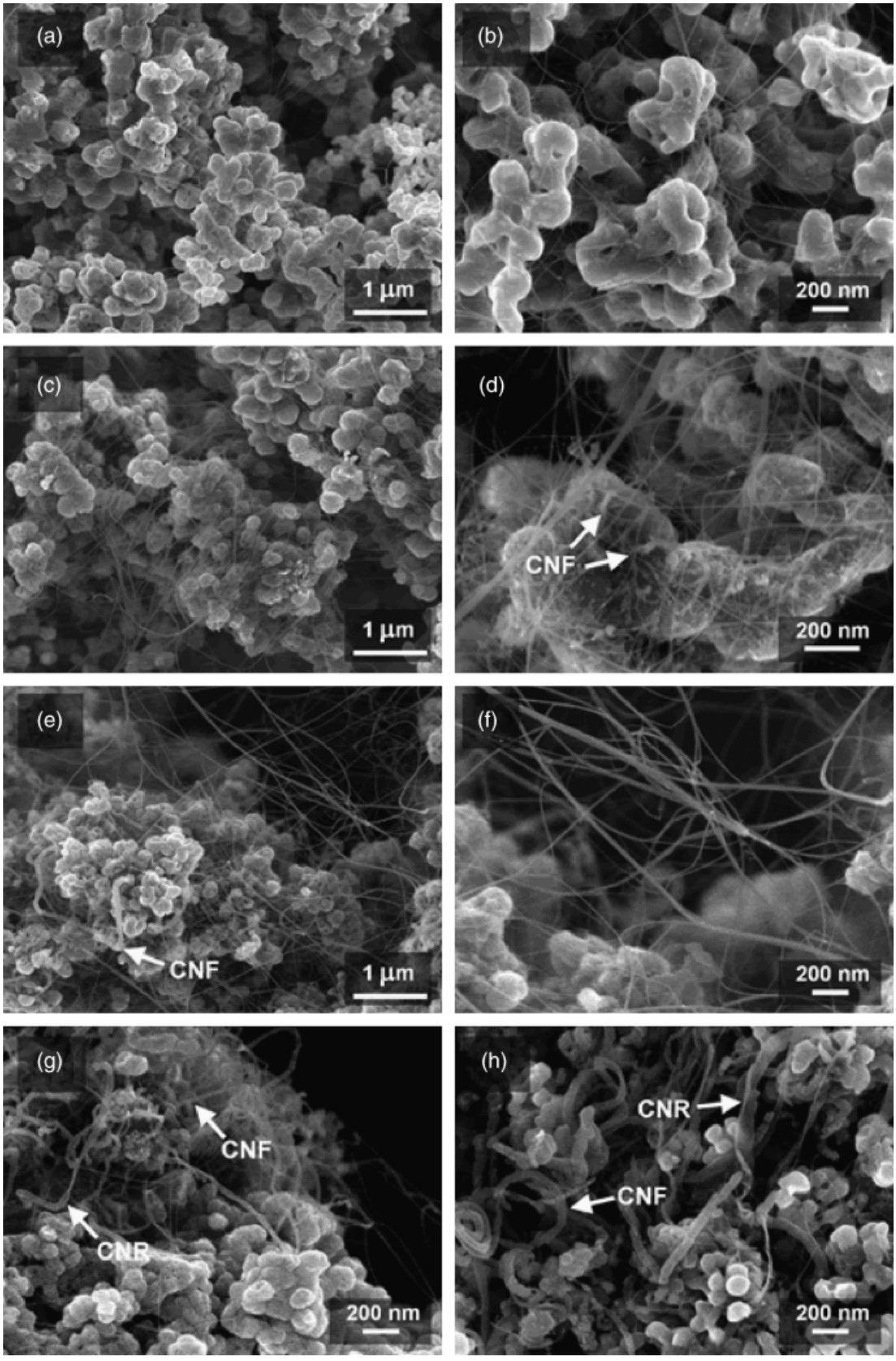

Fig. 3. FEG-SEM micrographs of the carbon nanotube–Fe–Al_2O_3 nanocomposite powders showing the carbonaceous materials formed over the powders during the catalytic chemical vapor deposition process: **(**a,b**)** R–5Fe1070T60t, **(**c,d**)** R–7Fe1060T60t, **(**e,f**)** R–10Fe1000T30t, (g) R–10Fe1000T1t, and **(**h**)** R–10Fe1050T60t. Arrows point to carbon nanofibers (CNF) and carbon nanoribbons (CNR).

after oxidation (11.0 m^2/g) is three times smaller than that of the corresponding starting oxide powder (32.9 m^2/g).

When S_o is subtracted from S_n, the obtained ΔS value (Table I) shows the SSA of carbon per gram of the nanocomposite powder, which corresponds mainly to the surface area of CNTs, because it is considered that other forms of carbon (particularly CNFs and CNRs) are in minor quantity and/or have much smaller SSA than CNTs.[6] Therefore, ΔS value represents

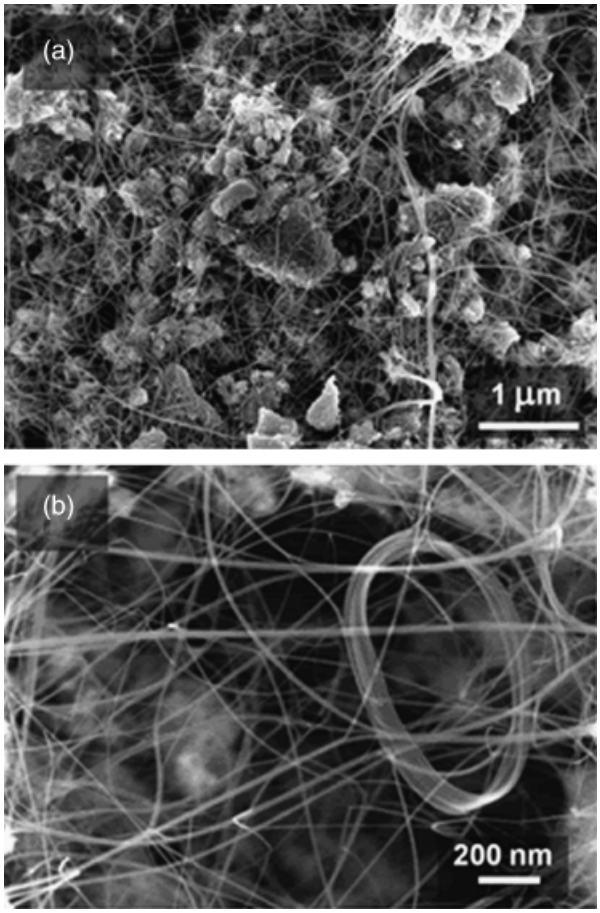

Fig. 4. FEG-SEM images of the R–CS nanocomposite powder. (a) Lower magnification image shows the carbon nanotubes (CNTs) covering the matrix grains evenly, (b) higher magnification image focuses on flexible CNTs bundles.

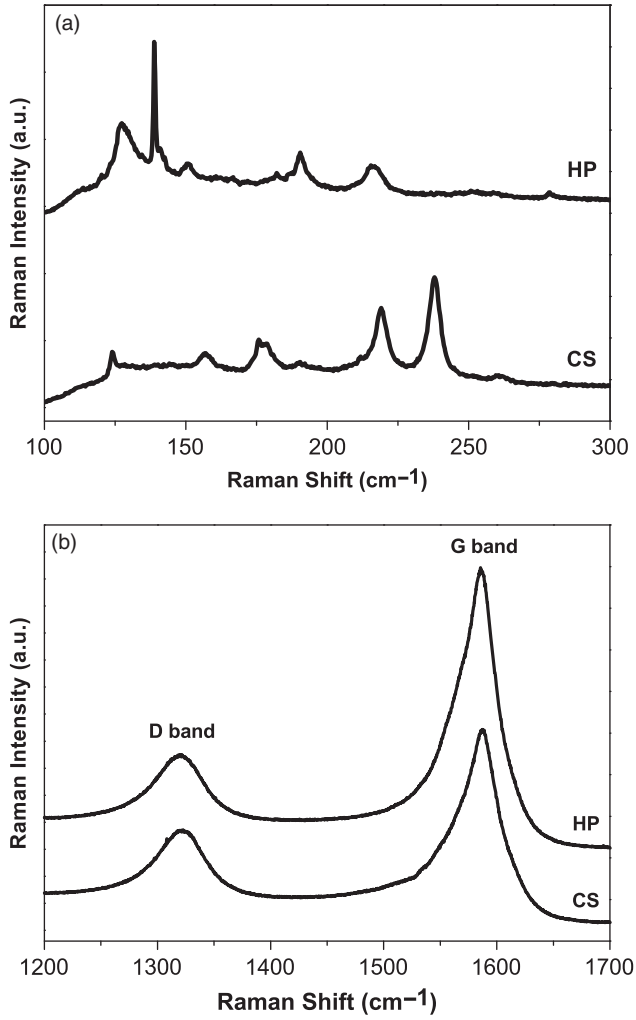

Fig. 5. Raman spectra of the carbon nanotube–Fe–Al_2O_3 nanocomposites prepared from the 10Fe1000T30t powder (HP) and 10 cat.% Fe-doped combustion-synthesized Al_2O_3 powder (CS). (a) Low-frequency region and (b) high-frequency region of the Raman spectra.

the quantity of CNTs or CNT bundles in the nanocomposite powder.[6] ΔS calculations revealed that among the homogeneously precipitated powders, the highest CNTs quantities were achieved with the 10 cat.% Fe-doped powders, especially for the R–10Fe1000T30t (30.9 m^2/g). This result is in agreement with the SEM observations of the nanocomposite powders (Figs. 3(a), (c), and (e)). It was also observed that the ΔS value of the R–CS system (37.6 m^2/g) is higher than the nanocomposites prepared from the homogeneously precipitated powders.

$\Delta S/C_n$ (Table I), which represents the CNTs quality, corresponds to the SSA of carbon if it is assumed that the SSA of the other species remains almost constant during the nanocomposite oxidation.[6] Higher $\Delta S/C_n$ value means smaller average tube diameter and/or tubes with fewer walls and/or more carbon in tubular form.[6] In homogeneously precipitated powder systems, this parameter ranges from 143–356 m^2/g, including the experimental uncertainty. The highest $\Delta S/C_n$ value among these systems is calculated as 329 ± 27 m^2/g for the R–10Fe1000T30t. For the R–CS system, this CNTs quality value is 459 ± 31 m^2/g (Table I).

Figure 5 shows the Raman spectra of the R–10Fe1000T30t and R–CS nanocomposite powder systems. The intense bands observed in the low-frequency range (100–300 cm^{-1}) of the Raman spectrum are assigned to the radial breathing modes (RBM),[18] which correspond to the atomic vibration of C atoms in the radial direction, as if the tube was breathing.[19] Each RBM signs the presence of a specific tube diameter in the sample according to the relations between the RBM frequency and the tube diameter.[18] In Fig. 5(a), the RBM peaks are observed for both samples, suggesting that at least a part of the CNTs have only few walls. The diameters, which are calculated from the frequency of the RBM peaks,[20] are in the ranges 1.02–1.76 and 0.83–1.83 nm for the R–10Fe1000T30t and R–CS nanocomposite powders, respectively. However, it should be noted that it is not possible to scan all the diameters of the CNT population in the sample with only one wavelength because a specific excitation wavelength enhances the signal for only some of the CNTs.[21] The high-frequency region of the Raman spectra shows the so-called D-band ($\sim$1320 cm^{-1}) and the G-band ($\sim$1586 cm^{-1}) (Fig. 5(b)). The D-band to G-band intensity ratio ($I_{D/G}$) is 26% for the R–10Fe1000T30t and 35% for the R–CS nanocomposite powder. D-band is induced from disorder in graphitic materials and the G-band originates from the tangential vibrations of sp^2 carbon atoms along the tube axis.[19] The $I_{D/G}$ ratio is commonly used to characterize different kinds of disordered sp^2 carbon (e.g, carbon fibers)[22] and an increasing $I_{D/G}$ value is generally attributed to the presence of more structural defects. Therefore, the measured $I_{D/G}$ values suggest that the R–10Fe1000T30t system contains fewer amounts of undesired carbon phases (CNFs or CNRs and/or disorganized carbon) with respect to the R–CS.

TEM images of the R–10Fe1000T30t and R–CS nanocomposite powders (Fig. 6) show that both samples contain isolated CNTs, 1–5 nm in diameter and CNTs bundles, about 10 nm in diameter, i.e. composed of only few CNTs. Some CNFs have been marginally detected in the R–10Fe1000T30t, as in agreement with the SEM observations, but also in the R–CS for which such a carbon form has not been evidenced by SEM, but suggested by the Raman spectroscopy.

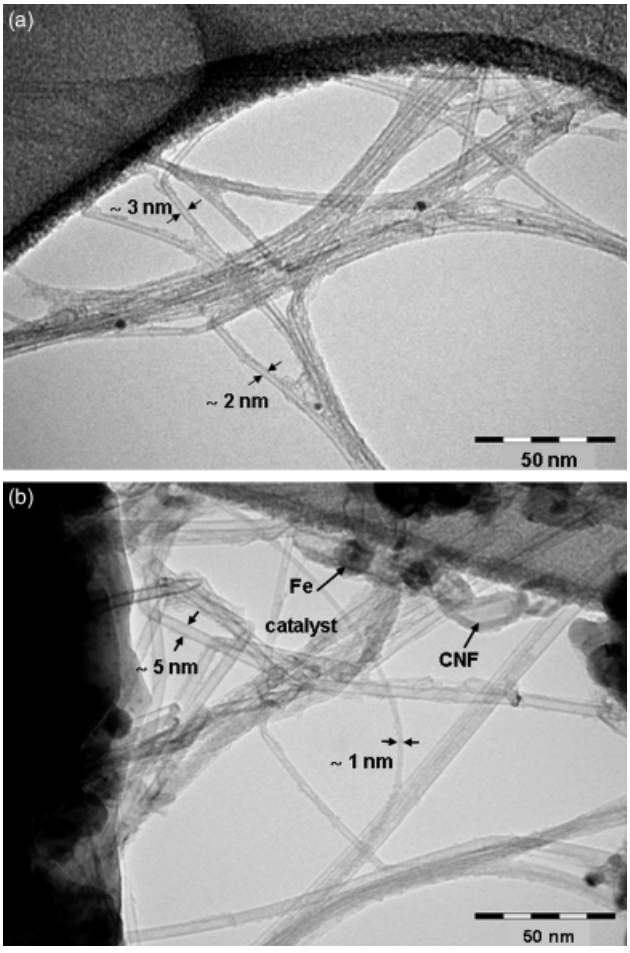

Fig. 6. TEM images of carbon nanotube (CNT)–Fe–Al_2O_3 nanocomposites prepared from (a) 10Fe1000T30t powder, and (b) from 10 cat.% Fe-doped combustion-synthesized Al_2O_3 powder (CS). Arrows indicate the diameters of individual CNTs, large Fe catalyst nanoparticles and carbon nanofibers.

IV. Discussion

The XRD pattern of the CS powder synthesized by the combustion route and calcined at 1100°C, 20 min showed that this powder crystallized in the monophased α-$Al_{1.8}Fe_{0.2}O_3$ form; however, a complete transformation into the α-form without any transition Al_2O_3 and/or hematite-rich secondary phase could not be achieved for 7 and 10 cat.% Fe-doped alumina powders prepared by homogeneous precipitation of hydroxides even after calcination. Muan and Gee[23] reported that ~10 mol% hematite was the maximum dopant amount for retaining a monophased powder at temperatures below 1318°C. The XRD data obtained in the present study suggest that this maximum amount may vary depending on the synthesis route, which is in agreement with the previous studies.[6–9,12,13] Among the homogeneously precipitated powders, only the 5Fe1070T60t system is free from the α-Fe_2O_3 and transitional Al_2O_3 phases. No CNF was detected in the SEM analysis of the corresponding nanocomposite powder (R–5Fe1070T60t). A few CNFs were detected in the R–7Fe1060T60t and R–10T1000T30t nanocomposites, the corresponding oxides of which contain low amount of hematite-rich secondary phase. The amount of defective structures (CNFs and CNRs) in the nanocomposites increased, when the corresponding oxides contained higher amount of α-Fe_2O_3 and/or transitional Al_2O_3 phase. For the R–10Fe1050T60t, the higher CNFs and CNRs content is correlated with higher quantity of hematite-rich secondary phase in the starting oxide powder. Peigney *et al.*[8] reported that α-Fe_2O_3 phase segregation causes formation of too large Fe nanoparticles and consequently, result in the formation of CNFs. For the R–10Fe1000T1t, large aggregates of CNFs and CNRs could have been catalyzed by large Fe nanoparticles (diameter >5 nm) formed probably during the CCVD process due to the presence of transitional alumina in the starting oxide powder. Laurent *et al.*[7] reported that larger catalyst nanoparticles were formed in the presence of amorphous or transition compounds due to coalescence of very small nanoparticles during the CCVD process which then leads to formation of inactive catalysts or CNFs, as in agreement with the results obtained in the present study.

The amount of carbon deposited during the CCVD is prone to increase with increasing Fe content, because higher amount of Fe means more catalytic nanoparticles.[8] Moreover, it has been shown that Fe nanoparticles are formed both within and at the surface of the alumina grains, and only the nanoparticles located at the surface immediately act as catalyst for the formation of CNTs.[6] Therefore, a very high SSA is desired, because it enhances the proportion of Fe nanoparticles located at the particle surface and thus increases the quantity of CNTs.[9] However, the C_n values do not show a clear correlation with neither the Fe content nor the SSA values of the oxide powders (S_i) in the present work. The SEM results suggest that the high carbon content in the R–10Fe1000T1t (13.9 wt.%) and R–10Fe1050T60t (12.4 wt.%) can be attributed to the presence of significant amounts of CNFs and CNRs in these two powders because one of these filaments contains much more carbon than that a CNT or a bundle of CNTs can contain.

Because the C_n value includes all the carbon species deposited during the CCVD, it would be more meaningful to interpret this value by combining it with the SSA of the nanocomposite powder in order to extract quantitative information about only CNTs. The severe increase in the SSA of the powders after being subjected to the CCVD (S_n, Table I) indicates that a considerable amount of the carbon was deposited in the form of CNTs. The carbon is deposited especially in the form of CNTs upon the CCVD as long as the requirements for a successful CNTs synthesis are satisfied.[7–9] The contribution of Fe and Fe_3C particles, which form at the surface of the matrix grains, to the increase in the SSA is expected to be at much smaller extent with respect to the contribution from CNTs.[24] The SSA of oxidized powders are expected to be similar or slightly lower than their S_i values, as reported by Laurent *et al.*[9]; however, the SSA values of the R–10Fe1000T1t, R–10Fe1000T30t, and R–5Fe1070T60t powders after oxidation are lower than the initial surface area of their corresponding starting oxides. For the R–10Fe1000T1t, this could be due to crystallization of the remaining transition Al_2O_3 into the stable α-form during the CCVD operated at 1000°C and/or during the oxidation at 900°C (local temperature is expected to be higher than 900°C due to the combustion process). Moreover, the decrease in SSA of the R–10Fe1000T30t and R–5Fe1070T60t powders may arise from the neck formation between fine particles during the CCVD and/or the oxidation treatment. The SSA of the R–CS after oxidation (11.0 m^2/g) is much lower than the initial SSA (32.9 m^2/g) of the CS powder, in comparison to the other nanocomposite and corresponding oxide powders. Because no transitional Al_2O_3 phase has been detected in the CS powder, this significant reduction in SSA may be due to sintering of the oxide particles, particularly the most reactive, i.e. the smaller ones whom the diameter is below 100 nm, during CCVD and/or oxidation. Therefore, although the maximum CNTs quantity (ΔS, 37.6 m^2/g) was measured for the R–CS nanocomposite powder, this value probably includes the decrease in SSA due to sintering effect besides the SSA of CNTs and hence it may be misleading. Therefore, the quantity of CNTs could be lower than the value calculated based on the ΔS value. Moreover, the CNT quality of the R–CS system is probably much lower than that the predicted $\Delta S/C_n$ value (459 ± 31 m^2/g) due to the same reason. Therefore, $\Delta S/C_n$ is not very representative of the quality of CNTs for the R–CS. The R–10Fe1000T30t has a higher quality parameter ($\Delta S/C_n = 329 \pm 27$ m^2/g) than the other CNTs–Fe–Al_2O_3

nanocomposites prepared from homogeneously precipitated powders, in spite of the observation of a few CNFs in this sample. The quantity parameter was also very high ($\Delta S = 30.9 \pm 1.9$ m^2/g) for this sample. If these results are compared with the previously reported results,[6–9] where the maximum achieved quality and quantity parameters were 314 m^2/g[9] and 19.6 m^2/g,[9] respectively, it is obvious that the results obtained in this study are superior. It should be also noted that in the previous work where the best results were reported,[9] the SSA of the starting oxide was only 8.1 m^2/g and the CCVD treatment was operated at 1050°C (50°C higher than the present work). It is known that a higher temperature always favours the deposition of a higher quantity of carbon.

The Raman and TEM analyses revealed the presence of CNFs in the R–CS system, although this carbon form has not been observed by SEM. Thus, although a hematite-rich secondary phase was not revealed by XRD for the corresponding starting oxide (CS), such a phase may still exist at a content below the detection threshold of this technique and result in the production of large Fe nanoparticles (> 5 nm) (Fig. 6(b)) which catalyze the growth of a few CNFs.

Consequently, the starting oxide powder containing 10 cat.% Fe, obtained by homogeneous precipitation of hydroxide and the optimized calcination (1000°C for 30 min) allows synthesis of much higher quantity of CNTs *in situ* within the alumina matrix, while providing a better quality with respect to the previous studies.[6–9] Raman results support that the quality of the CNTs, grown over 10Fe1000T30t, is better than that of the combustion-synthesized powder.

In the present work, one of the main advantage of the starting oxide powders (α-$Al_{2-2x}Fe_{2x}O_3$) prepared by the homogeneous precipitation method followed by a calcination treatment is their higher SSA (19–34 m^2/g—Table I) when compared with the catalytic materials prepared by other chemical routes, also followed by a calcination treatment (< 10 m^2/g).[6–9,12] Therefore, there is no need for milling and subsequently no potential of contamination. As in previous works, the main key is to find the appropriate calcination treatment (temperature and time) for the starting oxide powder with as high Fe content as possible to assure its complete crystallization under the corundum form while minimizing the amount of the hematite-rich secondary phase and maximizing the SSA. The consequence is the preparation, by the CCVD treatment, of a higher quantity of CNTs with a reasonable quality, i.e. only very few CNFs, as shown for the R–10Fe1000T30t nanocomposite powder, the corresponding oxide powder of which was calcined at 1000°C for 30 min, giving a SSA of 19.1 m^2/g.

V. Conclusions

The results of this study show that nanosized Fe-doped alumina particles (α-$Al_{2-2x}Fe_{2x}O_3$) produced by the homogeneous precipitation of hydroxides are viable catalytic materials for the *in situ* synthesis of homogeneously distributed CNTs in the Fe–Al_2O_3 matrix. One of the main advantages of the homogeneous precipitation and subsequent calcination process against to the combustion synthesis and other commonly practiced chemical routes is that physical and chemical characteristics of the Fe-doped Al_2O_3 powders can be tailored, which enables one to control the quality and quantity of CNTs during CCVD process. The homogeneously precipitated powders exhibit high SSA even after calcination and hence there is no need for milling and subsequently no potential of contamination. The calcination treatments of the starting oxides with high Fe contents (7 or 10 cat.%) must be optimized (temperature and time) to keep the SSA of the powder as high as possible while limiting the phase partitioning of the corundum form. Accordingly, the monodispersed homogeneously synthesized powders, particularly that containing 10 cat.% Fe content in the starting oxide, and their much higher SSA than similar catalytic materials prepared by other chemical routes result in the *in situ* synthesis of larger quantities of CNTs with good quality in the nanocomposite powders.

Acknowledgment

One of the authors, E. Suvaci, thanks Turkish Academy of Sciences (TUBA) for financial support through Outstanding Young Investigator Award (GEBIP) Programme.

References

[1]M. S. Dresselhaus, G. Dresselhaus, and P. C. Eklund, *Science of Fullerenes and Carbon Nanotubes*. Academic Press, San Diego, 1995.
[2]J. Robertson, "Realistic Applications of CNTs," *Mater. Today*, **7**, 46–52 (2004).
[3]N. P. Padture, "Multifunctional Composites of Ceramics and Single-Walled Carbon Nanotubes," *Adv. Mater.*, **21**, 1767–70 (2009).
[4]J. Cho, A. R. Boccaccini, and M. S. P. Shaffer, "Ceramic Matrix Composites Containing Carbon Nanotubes," *J. Mater. Sci.*, **44**, 1934–51 (2009).
[5]L. Waisman, H. D. Wagner, and G. Marom, "The Role of Surfactants in Dispersion of Carbon Nanotubes," *Adv. Colloid Interface Sci.*, **128–30**, 37–46 (2006).
[6]A. Peigney, Ch. Laurent, F. Dobigeon, and A. Rousset, "Carbon Nanotubes Grown *In-Situ* by a Novel Catalytic Method," *J. Mater. Res.*, **12**, 613–5 (1997).
[7]Ch. Laurent, A. Peigney, and A. Rousset, "Synthesis of Carbon Nanotube–Fe–Al_2O_3 Nanocomposite Powders by Selective Reduction of Different $Al_{1.8}Fe_{0.2}O_3$ Solid Solutions," *J. Mater. Chem.*, **8**, 1263–72 (1998).
[8]A. Peigney, Ch. Laurent, O. Dumortier, and A. Rousset, "Carbon Nanotubes–Fe–Al_2O_3 Nanocomposites. Part I: Influence of the Fe Content on the Synthesis of Powders," *J. Eur. Ceram. Soc.*, **18**, 1995–2004 (1998).
[9]Ch. Laurent, A. Peigney, E. Flahaut, and A. Rousset, "Synthesis of Carbon Nanotubes–Fe–Al_2O_3 Powders. Influence of the Characteristics of the Starting $Al_{1.8}Fe_{0.2}O_3$ Oxide Solid Solution," *Mater. Res. Bull.*, **35**, 661–73 (2000).
[10]J. L. McArdle and G. L. Messing, "Transformation and Microstructure Control in Boehmite-Derived Alumina by Ferric Oxide Seeding," *Adv. Ceram. Mater.*, **3**, 387–92 (1988).
[11]P. Tartaj and J. Tartaj, "Preparation, Characterization and Sintering Behavior of Spherical Iron Oxide Doped Alumina Particles," *Acta Mater.*, **50**, 5–12 (2002).
[12]V. G. De Resende, E. De Grave, A. Cordier, A. Weibel, A. Peigney, and C. Laurent, "Catalytic Chemical Vapor Deposition Synthesis of Single- and Double-Walled Carbon Nanotubes from α-$(Al_{1-x}Fe_x)_2O_3$ Powders and Self-Supported Foams," *Carbon*, **47**, 482–92 (2009).
[13]A. Cordier, A. Peigney, E. D. Grave, E. Flahaut, and Ch. Laurent, "Synthesis of the Metastable α-$Al_{1.8}Fe_{0.2}O_3$ Solid Solution from Precursors Prepared by Combustion," *J. Eur. Ceram. Soc.*, **26**, 3099–111 (2006).
[14]A. E. Nielsen, *Kinetics of Precipitation*. Pergamon Press, Oxford, 1969.
[15]E. Flahaut, A. Peigney, Ch. Laurent, and A. Rousset, "Synthesis of Single-Walled Carbon Nanotube–Co–MgO Composite Powders and Extraction of the Nanotubes," *J. Mater. Chem.*, **10**, 249–52 (2000).
[16]E. Flahaut, A. Peigney, and Ch. Laurent, "Double-Walled Carbon Nanotubes in Composite Powders," *J. Nanosci. Nanotech.*, **3**, 151–8 (2003).
[17]A. R. West, *Solid State Chemistry and Its Applications*. Wiley, Chichester, U.K., 1984.
[18]L. Alvarez, A. Righi, S. Rols, E. Anglaret, and J. L. Sauvajol, "Excitation Energy Dependence of the Raman Spectrum of Single-Walled Carbon Nanotubes," *Chem. Phys. Lett.*, **320**, 441–7 (2000).
[19]A. Jorio, M. A. Pimenta, A. G. Souza Filho, R. Saito, G. Dresselhaus, and M. S. Dresselhaus, "Characterizing Carbon Nanotube Samples with Resonance Raman Scattering," *New J. Phys.*, **5**, 139.1–17 (2003).
[20]S. Bandow, S. Asaka, Y. Saito, A. M. Rao, L. Grigorian, E. Richter, and P. C. Eklund, "Effect of the Growth Temperature on the Diameter Distribution and Chirality of Single-Wall Carbon Nanotubes," *Phys. Rev. Lett.*, **80**, 3779–82 (1998).
[21]E. Flahaut, Ch. Laurent, and A. Peigney, "Catalytic CVD Synthesis of Double and Triple-Walled Carbon Nanotubes by the Control of the Catalyst Preparation," *Carbon*, **43**, 375–83 (2005).
[22]W. H. Weber and R. Merlin, *Raman Scattering in Materials Science*. Springer-Verlag, New York, 2000.
[23]A. Muan and C. L. Gee, "Phase Equilibrium Studies in the System Iron Oxide–Al_2O_3 in Air and at 1 atm. O_2 Pressure," *J. Am. Ceram. Soc.*, **39**, 207–14 (1956).
[24]A. Peigney, Ch. Laurent, and A. Rousset, "Influence of the Composition of a H_2–CH_4 Gas Mixture on the Catalytic Synthesis of Carbon Nanotubes–Fe/Fe_3C–Al_2O_3 Nanocomposite Powders," *J. Mater. Chem.*, **9**, 1167–77 (1999). □